PAPER 134 – EXPERIMENTAL EVALUATION AND OPTIMIZATION OF ORGANIC MATERIALS FOR THE DEVELOPMENT OF FREE-ASBESTOS BRAKE PADS

AElakhame Z. Uwagbai[1], Shuaib–Babata Y. Lanre[2], Busari O. Yusuf[2], Ajao K. Suleiman[2]

[1]Department of Prototype Design and Development, Federal Institute of Industrial Research, Oshodi, Lagos, Nigeria.
[2]Department of Minerals and Metallurgical Engineering, Faculty of Engineering, University of Ilorin, Kwara, Nigeria.
*Email: ezeberu@yahoo.com

ABSTRACT
This study presents evaluation and optimization of locally available organic materials for the development of asbestos free brake pads. Some eco-friendly materials for automobile brake pads selected locally are rice husk fibres, gum Arabic, graphite, quartz and steel dust were processed and evaluated for possible asbestos replacement in comparison with the commercial brake pad materials. The material was processed and characterised for elemental composition, microstructural analysis phase presents and observe chemical properties. Using scanning electron microscope (SEM) equipped energy dispersive x-ray spectroscopy (EDX), x-ray diffractometer (XRD) spectrometer and Fourier transform Infrared Spectrophotometer (FTIR) respectively. Commercial brake pad XRD spectrum consist of three compounds exhibit a sharp, tight peak and wagging movement to attest that, the compounds are crystallite and amorphous. While, all the selected materials are also crystallite, excluding gum Arabic and rice husk that are amorphous. Characterization of SEM-EDX shows that, the commercial brake pad has similar element composition with the selected reinforcement materials, except barium oxide find out to be the based materials in the commercial brake pad that was alternatively replaced by rice husk in the new laboratory formulation. Also, it was determined that FTIR analysis of the commercial brake pad has common functional group of 1, 3 – disubstitution (meta) (C-H), alkyl-substituted ether (C – O) stretch, skeletal (C-C) vibrations aromatic tertiary amine (CN) stretch and vinyl (C-H) in-plane bend molecules with the selected materials for new laboratory formulation. Hence, this is accentuating that, the materials can be alternative use for production. It can be finally concluded that the locally available raw materials selected has been evaluated with higher quality than the existing properties of the commercial brake pad which can definitively leads to its low cost of its production.

KEYWORDS: Brake pad; Microstructure; Rice Husk; Scanning Electron Microscope; Asbestor

1. INTRODUCTION

Brake pads is an essential component of the braking systems in automobiles to control the speed by converting kinetic energy of the vehicles to heat which is dissipated to the atmosphere. Brake pads are composed of steel backing plates with friction material bound to the surface that faces the disc brake rotor. (Bekir *et al*., 2022). Brake pad materials generally are classified into four principal categories, as Non-metallic materials, semi-metallic materials, fully metallic materials and ceramic materials. The requirements for friction material design includes stable friction force, reliable strength and good wear resistance over a wide range of braking condition. Moreover, the friction material must be compatible with a composite disc brake by forming reliable friction film (stable third-body layer) at the friction surface (Sathyamoorthy *et al*., 2022)

Composition of brake pads has rapidly changed, as a result of the ban on asbestos fibres and the heat being generated during braking causes reduction in braking efficiency (Durowaye et al., 2020). (Najmuddin *et al*., 2021). However, some less thermally stable resins in brake pads were identified as producing oily residues that contributed to brake fade (Abutu *et al*., 2018). All epoxy and certain phenolic resins were identified as evolving volatile gases during degradation causing a back pressure on the brake pad also resulting in brake fade (Heerok *et al*., 2021).

Recently, concerted effort to address environmental issues and the need to protect the environment has drawn research focus to the use of natural fibers in several applications, including brake pads (Najmuddin *et al*., 2021). Dalibor *et al*. (2022) evaluated palm kernel fibers (PKFS) for production of asbestos-free automotive brake pads and the findings concluded that PKF can be effectively used as replacement to asbestor. Nwogu *et al.*, (2021) studied physic-mechanical properties of basalt-based brake as alternative to ceramics brake pad following the standard procedures employed by commercial manufacturer and the result obtained showed that the properties of palm kernel shell-based brake pad wholly satisfied the recommendation of the Standard Organization of Nigeria (SON). Lawal *et al*. (2020) produced brake pad of agro based composits of cashew nut shells and Nigerian gum Arabic binder. The studied concluded that cashew nut shell can be used in placement of materials in commercial brake pad. Furthermore, the morphology and wear properties of palm ash and Polychlorinated Biphenyls (PCB)

waste brake pad further justify the potential of biomass (Ammar *et al.,* 2023). Also, was reported by Güney *et al.,* (2019). Performance evaluation of brake pads development using two different manufacturing methods employed for the design and production of asbestos free brake pad using cashew nutshell by Adekunle *et al.,* (2023). The results of the studies indicated that palm slag can be used effectively as an alternative to brake pad composites. Nwogu *et al.* (2021) embarked on microstructure and wear mechanisms investigation on the brake pad. The brake pad when compared with asbestos-based commercial brake pad they was found to perform effectively.
Hence, this work aimed at producing eco-friendly friction composite brake pads produced from local available raw materials and compare it with the commercial brake pad by using powder metallurgy method to develop samples for characterization.

2. MATERIALS AND METHODS

2.1. Materials

The raw composite materials used in this study were rice husk, quartz, steel slags, graphite and gun arabic were s ourced from Ofada, Ogun State; Okpila, Esako, Edo State; Africa Foundry, Ogijo, Shagamu, Ogun State; Sama-Borkono, Warji, Bauchi State; a local vendor within the industrial raw materials supplier trade group registered b ut were harvested in Kano State Nigeria respectively as shown in Figure 2.

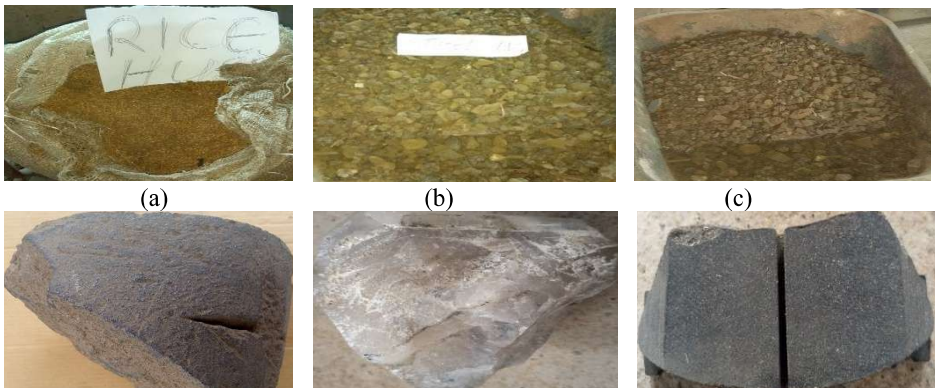

Fig 2: Photographs of raw materials (a) Rice Husk, (b) Gum Arabic, (c) Steel Slags, (d) Graphite ore, (e) Quartz ore and (f) Commercial brake pad

2.2. Materials Milling

A 5kg of the Rice Husk (HR) particles was sun dried for one week and charged into a ball milling machine (Model 87002 Limoges - France, A50 – 43, at 250 rpm) shown Figure 2b for 48 hours, with 25kg pebbles of different size (Dia 46.5mm, 39mm and 30mm of Big, medium and small) respectively; to form fine powder. The produced powder was later sieved with 75 µm (X), 100 µm (Y) and 150 µm (Z) sieve size aperture, using a vibro sieve machine (Vibro sieve machine Bs 410 standard sieves Endecotts Limited, London). While that of Steel slags, Quartz and graphite were pulverized using hammer mill, Model 000T, Puissance: 1.5KV, No 13634 (figure 2b) and then charged into milling machine to form fine powder and sieved to 100 µm particles size. The procedures were in line with the practice of Elakhame *et al.* (2020). The samples of the milled sieved materials are presented in Figure 3.

Fig 3: The various machines used and processed raw materials (a) Hammer Mill (b) Ball Milling Machine (c) Rice Husk (d) Processed Gum Arabic (e) Steel Slags (f) Graphite (g) Quartz.

2.3. Evaluation Properties of the raw Materials.

The elemental composition and phases present in the materials were determined with the accordance of ASTM standard.

I. **X-ray Diffractometer (XRD)**

XRD experiments were performed by (MiniFlex 600, Rigaku, Japan) diffractometer with Cu Kά based on ASTM E2860 – 20(2021)The experimental conditions were as follows: 45 kV, 40 mA, 21-23^{o}C, divergent beam slits 2 and 3 mm, receiving slits 1 and 0.2 mm, 2θ = 5-70^{O}C, and continuous scan with a scan rate of 2^{O}C/min.

II. **Scanning Electron Microscope and Energy Dispersive X-Ray Spectroscopy (SEM-EDS)**

The Scanning Electron Microscope with energy dispersive X-ray spectroscopy (SEM-EDS) (Phenom Prox model, phenomWorld, Eindhoven) based on test procedure in ASTM C1255 – 18(2018) and ASTM E2809 – 13(2019) Sample was placed on the Aluminium holder stub using sticky carbon tape. The sample was insulated using gold and then grounded electrically. The samples (each) where then labeled on their stub, then dried in the oven at 60^{O}C. Nitrogen line was opened at 50 psi and the vent button is pressed to fill the area with nitrogen for proper purging of the chamber.

III. **Fourier Transform Infrared Spectrophotometer (FTIR).**

For functional unit determination, the Fourier transform Infrared Spectrophotometer- (8400 S, Shimadzu, Japan) was used. Samples were weight-in at 0.01 g and homogenized with 0.01 g KBr anhydrous by mortar agate. The mixtures were pressed by vacuum hydraulic (Graseby Specac) at 1.2 psi to obtain transparency pellet. The procedure in American Society for Testing and Materials (ASTM) ASTM D6348 - 12(2020) standards were adopted to evaluate the raw materials.

3. RESULTS AND DISCUSSION

3.1. Elemental Compositions of the Raw Materials Specimens.

Table 1 shows the elemental composition of Commercial Brake Pad (CBP), Graphite (G), Quartz (Q), Steel Dust (SD), Rice Husk (RH) and Gum Arabic (GA)**.** The **results** revealed that the materials mainly contain metallics, semi-metallic and non-metals. It can be seen that G, Q, SS, RH & GA have similar composition of elements compared to the commercial specimen and equally found in asbestors. This suggested that the materials selected can be used as fibres in the development of brake pads. The amount of Fe, Ca, S, P, Mg and Na in G, Q, SS, RH and GA are comparable to the amounts present in the commercial specimen. All the raw materials have higher amounts of C and Si compared to the commercial specimen. Correspondingly, their properties are similar to commercial specimen, except the present of Ba only in the commercial specimen. These results are in lie with earlier confirmed by Durowaye *et al.* (2020).

Table 1: Comparison of EDX Results Showing Elemental Compositions of Commercial brake pad, graphite, quartz, steel dust, rice husk and Nig gum Arabic.

S/N	*Element Symbol*	*Element Name*	*CBP Weight Conc.*	*Graphite Weight Conc. (G)*	*Quartz Weight Conc. (Q)*	*Steel Slsg Weight Conc. (SS)*	*Rice Husk Weight Conc. (RH)*	*Gum Arabic Weight Conc. (GA)*
1	Ba	Barium	26.96	-			-	-
2	C	Carbon	19.51	74.06		5.24	49.21	55.52
3	Fe	Iron	17.46		1.47	33.53		-
4	Ca	Calcium	7.11	5.08	2.04	2.35	11.82	11.28
5	Ti	Titanium	5.83			0.56	0.42	0.74
6	S	Sulfur	5.07	1.29	0.78	0.44	3.83	1.56
7	Si	Silicon	3.58	8.01	76.72	52.07	16.83	3.18
8	Ag	Silver	3.48	3.12		1.14		-
9	K	Potassium	2.32	2.20	2.49	0.49	2.20	8.66
10	Mn	Manganese	2.14			1.61		-
11	P	Phosphorus	1.66	0.87	0.17	0.46	5.47	1.80
12	Mg	Magnesium	1.53	0.61	0.37	0.28	0.70	2.04

13	Al	Aluminium	1.27	2.51	3.58	1.25	1.51	-
14	V	Vanadium	1.14		0.30			-
15	Na	Sodium	0.57	0.31	0.22	0.07	0.22	0.37
16	N	Nitrogen	0.19	0.94			0.79	2.01
17	O	Oxygen	0.18	0.35			1.41	3.67
18	Cl	Chlorine	-	0.65				
19	**Ag**	Silver			4.51		2.34	6.07
20	**Y**	Yttrium			3.34		3.26	
21	**Cr**	Chromium			1.23	0.51		
22	**Zn**				2.75			

3.2. Scanning Electron Microscopy (SEM) of the Raw Materials Specimens.

In the spectrum of commercial specimen (Fig 4). It's evidenced that barium and iron powders are uniformly distributed in the resin. Graphite particles are evenly spread in the matrix. Clusters of Magnesium, Aluminum, Silica, Sulfur and other are seen at random locations Ossia *et al*. (2021). It is observed in Figure (4b) that silicon and calcium powders are distributed uniformly, while graphite particles are evenly spread in the matrix. Clusters of phosphorus, sulfur, yttrium, silver and aluminum are seen at random location (Yezhe *et al*., 2020).

The surface topography in (Figure 4c) was observed and the exterior surface of the gum arabic appears as irregular rocky surface and clearly different from that of the parent gum arabic, which has spherical shape with many dents on the surface (Nwogu *et al*., 2021). It is also observed that the spectrum had regular edges and homogenous structure (Figure 4d) (Oktem *et al*., 2021). The presence of large and spherical particles of silicon in (Figure 4e) indicate the rounded nature of quartz particles while the spherical grains indicate recycled nature and maturity of sediment accumulation. Quartz particle at higher magnification shows spongy surface and microcracks (Ahmad *et al*., 2021). (Figure 4f) shows that graphite has a wide and thick particle size indicated at 1000× magnification. The distance between the graphite particles looks wider with a far position and the existence of many stacks in the graphite structure indicating that graphite has a layered structure (Seckley, *et al*., 2020).

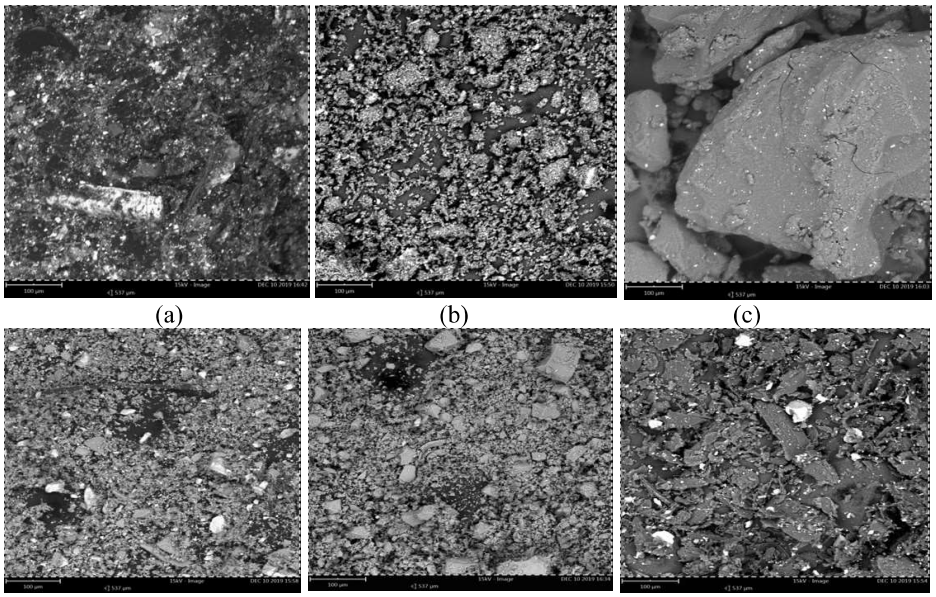

(a) (b) (c)

(d) (e) (f)

Fig 4: SEM micrograph of the samples (a) Commercial brake pad (b) Rice husk (c) Gum Arabic (d) Steel dust (e) Quartz (f) Graphite.

3.3 X-Ray Diffraction (XRD) Results of the Raw Materials Specimens.

The phase purity and crystallinity of the commercial pad was examined by X-ray diffraction techniques (XRD). Figure 5a consists of three phase compounds namely Graphite (C), Barite (BaO_4S) and Calcite ($Ca_6\ C_6\ O_{18}$). The

three compounds exhibit a sharp and tight peak at 2θ equal 20 and 30^{O} above 50% intensity Siburian *et al.* (2018). Figure 5b reveals that the optimal sharp peak occurred at 2θ angle equivalent 27^{O} with 100% intensity' the presences of sharp crystalline peaks all-round suggest that the graphite specimen is a predominantly crystallite (Obidiegwu *et al*., 2020). Figure 5c shows the amorphous nature of Nig gum arabic, the maximum intensity was obtained at 2θ angle equal 75^{O} Atmika *et al*. (2019). The absence of sharp crystalline peaks indicates that the specimen is amorphous in nature with an interesting feature of intensity distribution due to it wagging shape. Figure 5d consist of phase compound namely Quartz (Si_3C_6). The hexagonal crystal system exhibits a sharp and tight peak at 2θ equivalent 27^{O} with 100% intensity (Ammar *et al*, 2023). Figure 5e indicate the broad peaks at 2θ equals 75^{O} and low intensity counts confirmed the RH to be largely amorphous silica. Suggesting, the presence of quartz as crystalline phase. While Figure 5f shows the mineral phases of (silicon, graphite, magnetite, wuestite and ferdisillicite) were determined at higher and lower phases due to the very complex mineralogical composition of BOF steel slag, with many overlapping peaks and different solid solutions of oxides are (FeO, Fe_3O_4), silicon, Ferdicillicite (Fe) and graphite (Viderscak *et al.*, 2022). The purity crystal system exhibits a sharp and tight peak at 2θ equals 29^{O} with 100% intensity. This result shows that the steel slag is best suitable for thermal, abrasive and hardness enhancement properties in brake pad (Lyu *et al*., 2020).

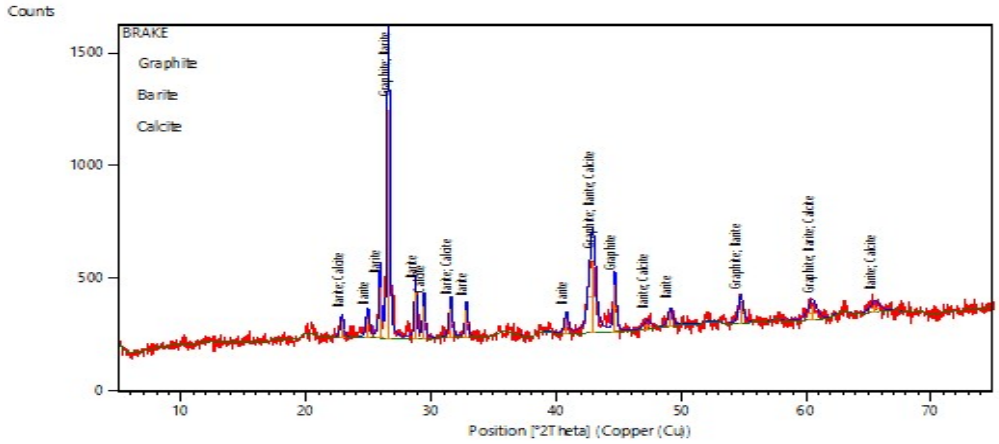

(a).

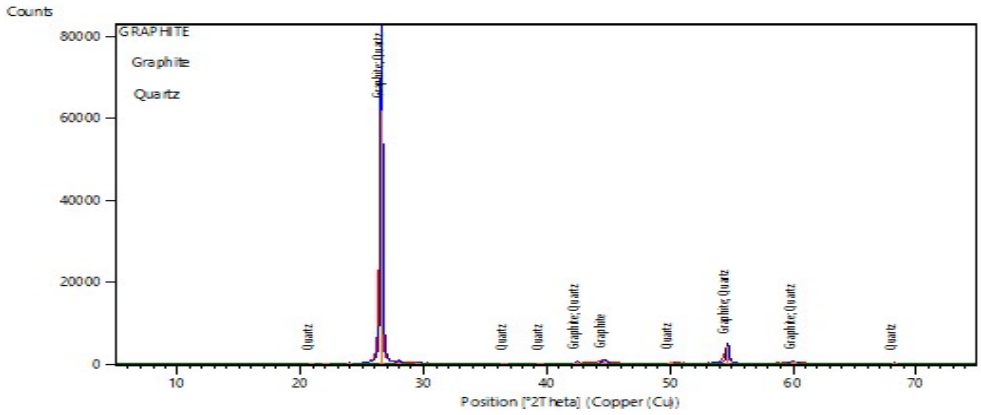

(b).

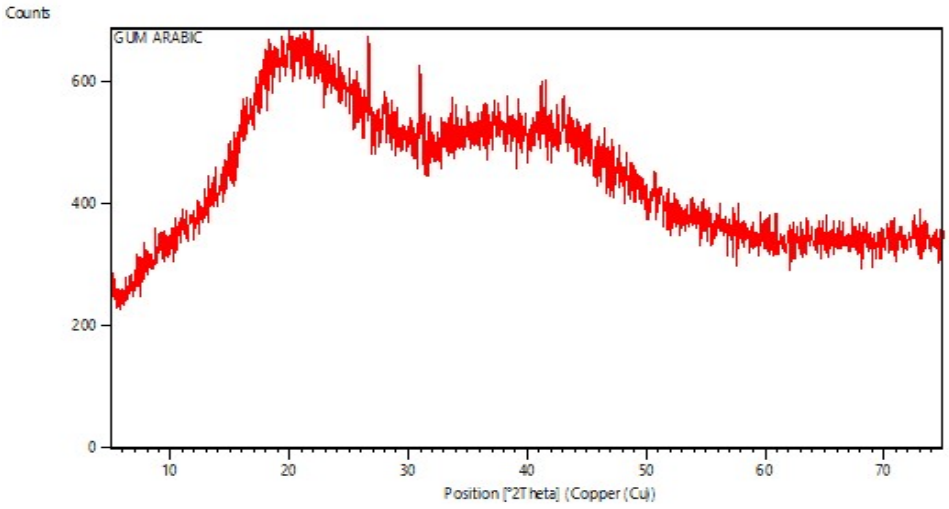
Counts
GUM ARABIC
600
400
200
0
10
20
30
40
50
60
70
Position [°2Theta] (Copper (Cu))

(c)

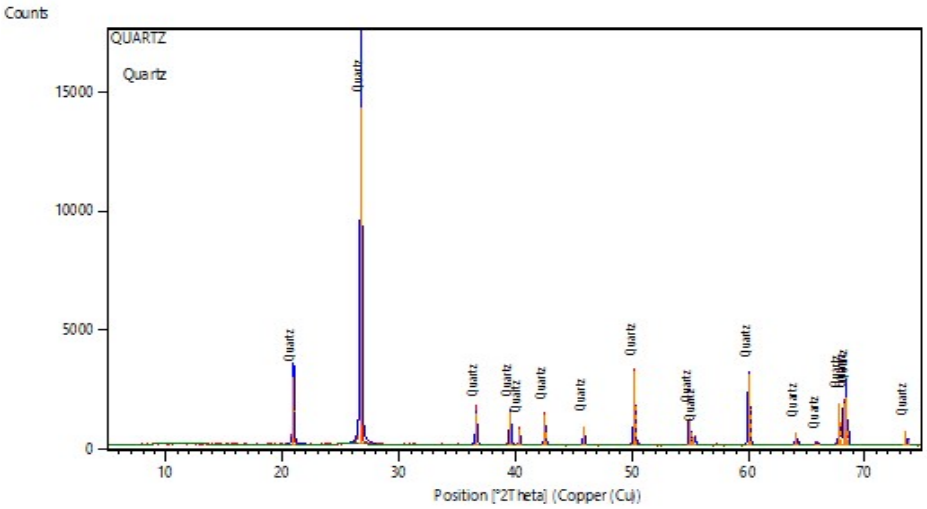
Counts
QUARTZ
Quartz
15000
10000
5000
0
Quartz
10
20
30
40
50
60
70
Position [°2Theta] (Copper (Cu))

(d)

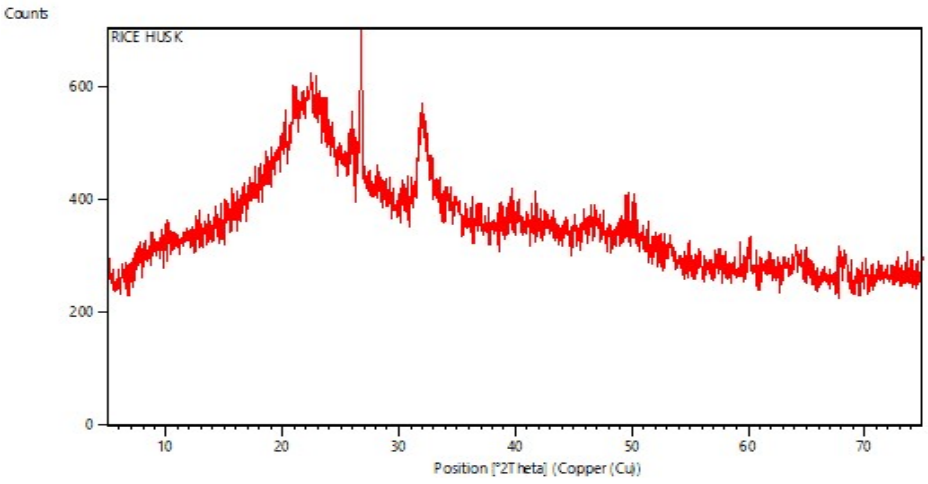
Counts
RICE HUSK
600
400
200
0
10
20
30
40
50
60
70
Position [°2Theta] (Copper (Cu))

(e)

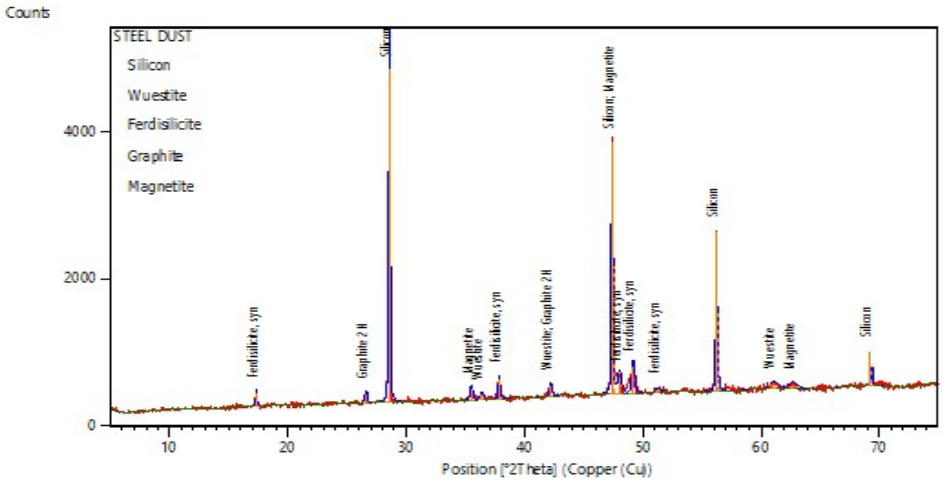

(f)

Fig 5. XRD spectrum of the samples (a) Commercial brake pad (CBP), (b) Graphite (c) Nig. Gum Arabic (d) Quartz (e) Rice husk (f) Steel dust.

3.4 Fourier Transform Infrared (FTIR) Spectrometer Results of the Raw Materials Specimens.

According to the peak values shown in Figure 6a the peaks at 887.28, 1419.66 and 2438.1 cm-^{1} band range show vinylidene (C-H) out of plane bend stresses in the structure. This indicates the presence of the CH molecule called Methylene. The peaks of organic silicone (Si-C-O) stretching at 3691 cm-^{1}indicate the presence of SiO_2 and SiC molecules in the structure Viderscak *et al*. (2022) and Heerok et al. (2021). Figure 6b shows finger print, peaks at 925.86, 1080.17 and 1388.79 cm-^{1} bands in the range of C-H and C-O indicate the presence of cyclohexane ring vibrations (C6-H12), cyclic ethers/large rings (CO_2CH_3) stretch and trimethyl or "tert-butyl" (multilplet) ($C_7H_{18}Sn$) molecules respectively (Oberdörster *et al*., 2005). The peak of 1535.39 and 1666.55 cm^{-1} bands corresponded to C-H-NO and N-H indicates the presence of aromatic nitro compounds ($C_6H_5NO_2$) and amide (NH_2) molecules respectively. The FTIR spectral of gum Arabic is displaced in Figure 6c. The peaks at finger print zone at 786.98, 1080.17, 1211.34, 1319.35 and1411.94 cm-^{1} bands in the range of C-H, C-O, P-O-C, C-N, C-H and C-H indicate the present of 1, 3 distribution (meta) ($C_6H_4N_2O_4$), cyclic ethers, large rings (CO_2CH_3) stretch, aromatic phosphates (PO_4) stretch, aromatic, aromatic tertiary amine (C3H6N) stretch and vinyl (CH_2) inter-plane bend molecules respectively (Lyu *et al*., 2020). According to the peak values of steel particles elements shown in Figure 6d, the peaks at 786.98, 1057.03, 1327.07 and 1411.94 cm-^{1} bands in the range of C-H, C-O, O-H and C-H indicate the presence of (CH) 1, 3 distribution (meta) ($C_6H_4N_2O_4$), alkyl-substituted ether (CHO_2) stretch, phenol or tertiary alcohol (R $_3$COH) bend, Vinyl (C6H6) in-plane bend molecules respectively (Güney *et al*., 2019). The FTIR spectral of quartz is shown in Figure 6e. The peaks of 786.98, 1057.03, 1226.77, 1319.35 and 1411.94 cm-^{1} bands in the range of C-H, C-O, C-C, C-N and C-H indicate the present of 1, 3 – disubstitution (meta) (C-H), alkyl-substituted ether (C – O) stretch, skeletal (C-C) vibrations aromatic tertiary amine (CN) stretch and vinyl (C-H) in-plane bend molecules respectively. The peaks of 1519.96, 1697.41 and 1797.72 cm-^{1} bands in the range of C-H, C-O, C-C, C-N and C-H indicate the present of aromatic nitro compounds ($C_6H_5NO_2$), aromatic combination bands (C_6H_6) and five – membered ring anhydride (C_4O) molecules respectively (Oktem *et al*., 2021). Figure 6f shown the peaks at 794.7, 887.28, 949.01, 1064.74, 1211.34, 1334.78, 1334.78 and 1411.94 cm-^{1} bands in the range of C-H, C-H, C-H, C-O, C-C, C-H, C-H and C-H, indicate the present of 1, 3-disubstitution (meta) (C-H), vinylidence (C-H) out of plane bend, cyclohexane ring vibrations (C_6H_{12}), alkyl-substituted ether C-O stretch, skeletal (C-C) vibrations, methyne (C-H) bend, methyne (C-H) bend, vinyl (C-H) in-plane bend molecules respectively Viderscak *et al*. (2022).

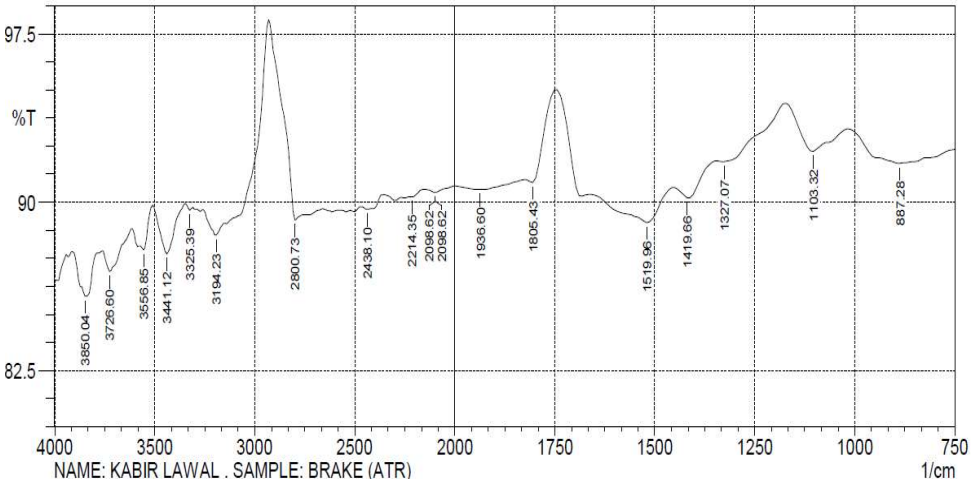
97.5
%T
90
82.5
3850.04
3726.60
3556.85
3441.12
3325.39
3194.23
2800.73
2438.10
2214.35
2098.62
2098.62
1936.60
1805.43
1519.96
1419.66
1327.07
1103.32
887.28
4000
3500
3000
2500
2000
1750
1500
1250
1000
750
NAME: KABIR LAWAL . SAMPLE: BRAKE (ATR)
1/cm

(a)

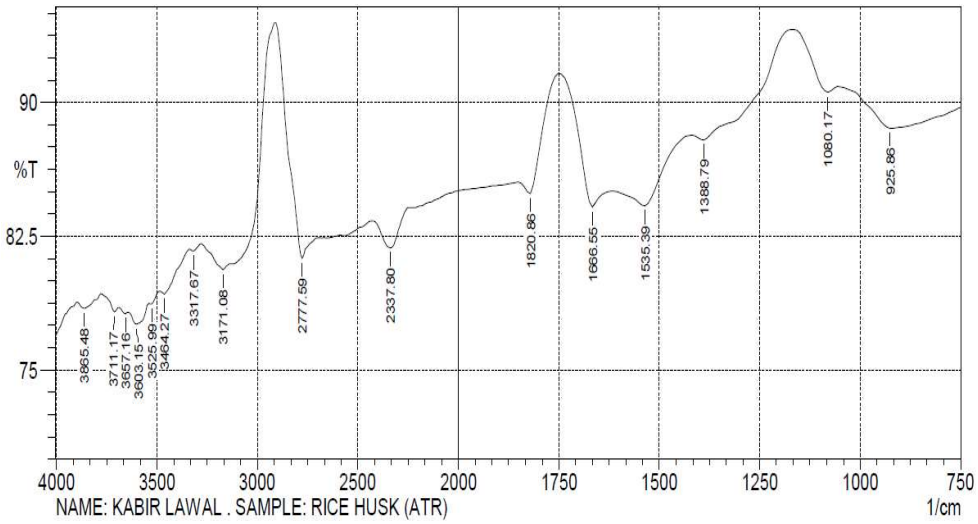
90
%T
82.5
75
3865.48
3711.17
3657.16
3603.15
3525.99
3464.27
3317.67
3171.08
2777.59
2337.80
1820.86
1666.55
1535.39
1388.79
1080.17
925.86
4000
3500
3000
2500
2000
1750
1500
1250
1000
750
NAME: KABIR LAWAL . SAMPLE: RICE HUSK (ATR)
1/cm

(b)

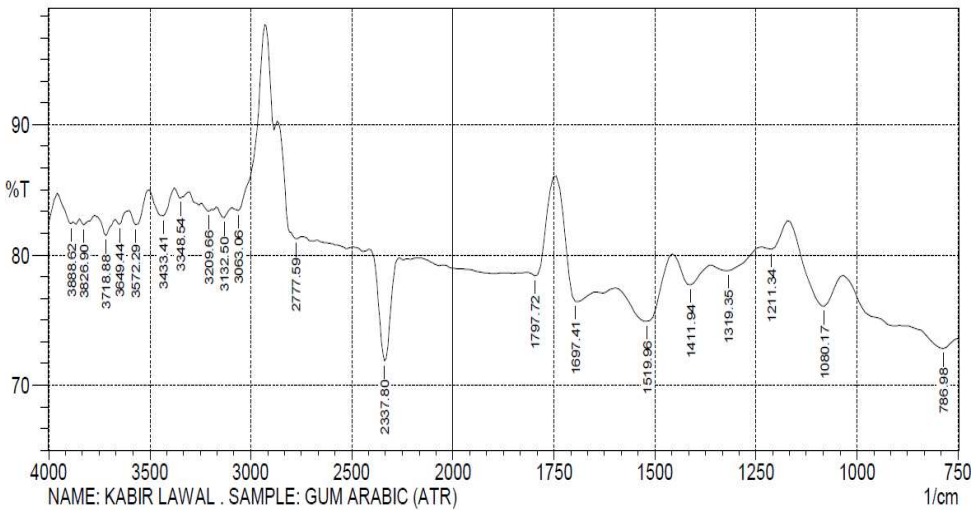
90
%T
80
70
3888.62
3826.90
3718.88
3649.44
3572.29
3433.41
3348.54
3209.66
3132.50
3063.06
2777.59
2337.80
1797.72
1697.41
1519.96
1411.94
1319.35
1211.34
1080.17
786.98
4000
3500
3000
2500
2000
1750
1500
1250
1000
750
NAME: KABIR LAWAL . SAMPLE: GUM ARABIC (ATR)
1/cm

(c)

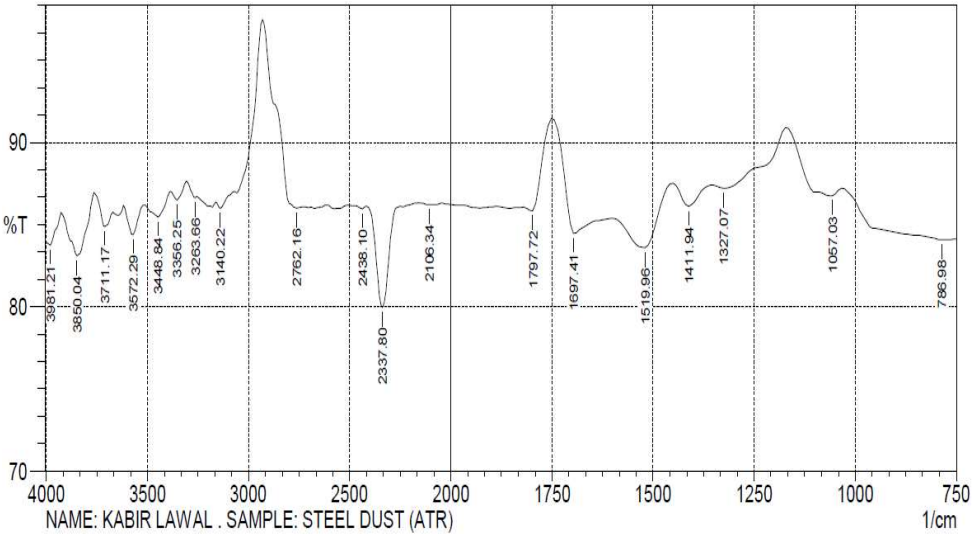

(d)

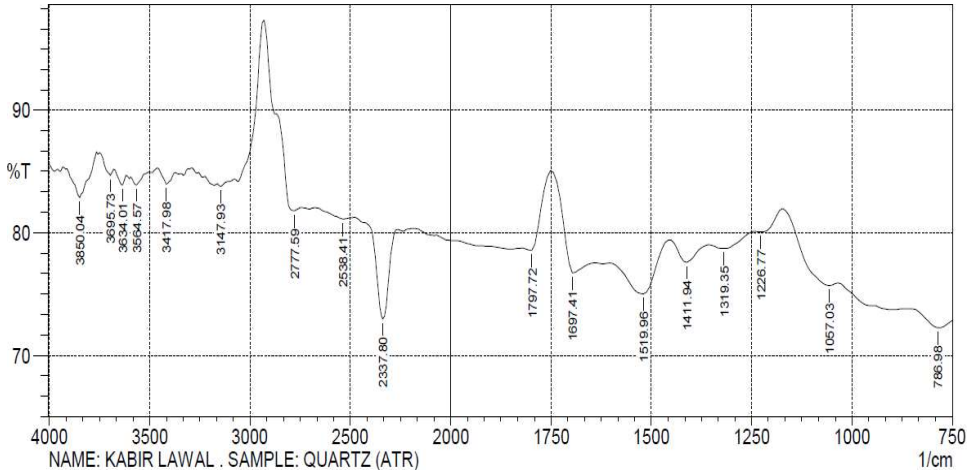

(e)

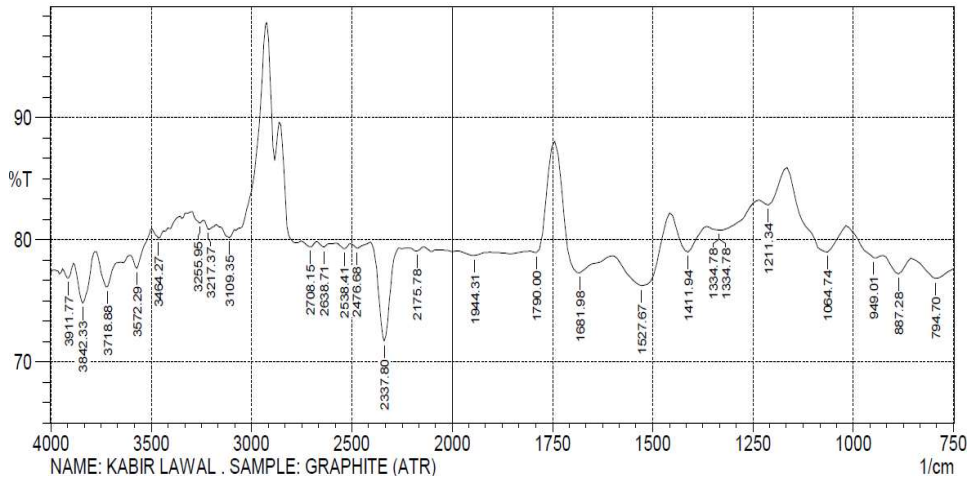

(f)

Fig. 6: FTIR spectrum of the samples (a) Commercial brake pad (b) Rice husk (c) Nig. Gum Arabic (d) Steel dust (e) Quartz (f) Graphite.

4 CONCLUSION

The evaluation of locally available raw materials selected for the development of brake pad were determined and the conclusions are summarized as follows:

1. That values of the necessary parameters obtained from the raw specimens are within the standard requirement for commercial specimen.
2. Chemical composition of all the raw material specimens exhibited most of the elements within the commercials specimen and even have higher wt% of C at Q (76.72)%, S.S (52.07)% and R.H (16.83)%; and Si at G (74.06)%, R.H (49.21)% and G.A (55.52)% compared to the commercial specimen at C (19.51)% and Si (3.58).
3. The spectrum of commercial specimen figure 3a exhibited uniformly distributed of both Barium and Iron in the resin and in comparison to the selected raw materials specimens that gave a better properties of evenly spread of particles in the matrix. Clusters of Magnesium, Aluminum, Silica, Sulfur, phosphorus, yttrium, silver and other are seen at random locations. Except, the surface topography in Figure 3c appeared as irregular rocky surface and clearly different from that of the parent gum Arabic with spherical shape and many dents on the surface. The presence of large and spherical particles of silicon in Figure 3e indicate the rounded nature of quartz particles.
4. The phase purity and crystallinity of the commercial specimen Figure 4a consists of three phase compounds namely Graphite (C), Barite (BaO_4S) and Calcite (Ca_6 C_6 O_{18}). The three compounds exhibited a sharp and tight peak at 2θ equal 20 and 30^O above 50% intensity, The selected raw materials specimens gave a better optimal sharp peak in Figure 4b at 2θ angle equivalent 27^O with 100% intensity; Figure 4c shows the amorphous nature of Gum Arabic, the maximum intensity was obtained at 2θ angle equal 75^O; Figure 4d exhibited a sharp and tight peak at 2θ equivalent 27^O with 100% intensity; Figure 4e indicate the broad peaks at 2θ equals 75^O and low intensity counts confirmed the RH to be largely amorphous silica. While Figure 4f exhibited a sharp and tight peak at 2θ equals 29^O with 100% intensity appropriately. This result shows that the steel slag is best suitable for thermal, abrasive and hardness enhancement properties in brake pad (Menezes *et al*., 2005).
5. FTIR analysis of the commercial brake pad has a common functional group of 1, 3 – disubstitution (meta) (C-H), alkyl-substituted ether (C – O) stretch, skeletal (C-C) vibrations aromatic tertiary amine (CN) stretch and vinyl (C-H) in-plane bend molecules which also displaced better in the selected materials for new laboratory formulation accentuating that, the materials
6. It can be finally concluded that the locally available raw materials selected has been evaluated with higher quality than the existing properties of the commercial specimen which can definitively leads to its low cost and can be alternative use for production.

REFERENCE

Achebe C.H, Chuckwuneke JL, Amone F.A and Ewulonu CMA Metrofit for abestor based brake pad employing Palm Kernel fibre as the base filler material, journal of material design and application. 7(27) (2018).

Adekunle n. o., ismaila s. o., kuye s. i., adetunji r., olamide o. o. and tomori o. design and production of asbestos free brake pad using cashew nutshell, lautech journal of engineering and technology 17 (1) 2023: 8-17.

Assoc. Prof. Nagwa Ahmed Elzayady, Ramadan Elsoeudy. Microstructure and Wear Mechanisms Investigation on the brake pad. Journal of Materials Research and Technology 11(5).(2021).

Atmika I.K.A, Subagia IDGA, Surata IW and Sutantra I.N Hardness and wear rate of basalt\ alumina in shellfish powder, reinforce phenolic rosin matrix hybrid composite brake lining pads. Material science and engineering 539{2019} 012012

Bekir Guney, Ibrahim Mutlie, Hanifi Kucuksariyildiz. The effect of flame spray coating on the tribological properties of Brake Disc. Journal of Polythenic, Volume: 23 Issue: 3, 755-761(2020).

C.U Ossia, Akuro Big- Alabo. Development and Characterization of Green Automotive Brake pads from waste shells of Giant African Snail (Achatina Achatina L.). International Journal of Advanced Manufacturin Technology. 114, 2887 – 2897(2021).

Dalibor Viderscak, Zdrauko Schauperl, Krunoslau Ormuz, Sanja Solic, Mladen Niksic, Drana Milcoc, Pavao Ormuz. Influence of Brake Pad Properties to Braking Characteristics. Promet-Traffic and transportation vol 34 No 1 (2022)

E.O. Obidiegwu, H.E. Mgbemere,E.F. Ochulor and P.A. Ajayi. Characterization of train brake blocks composite reinforced with aluminium dross. Nigerian Journal of Technology (NIJOTECH) Vol 39 No.4, October 2022.

Elakhame Z. U, Shuaib-Babata, Y. L, Jimoh S. O, Bankole L.K., Ambali, I.O., Production and Characterization of Asbestos Free Brake Pads From Kenaf Fiber Composite, Adeleke University Journal of Engineering and Technology [AUJET] Vol. 3, No 1, 69-78 (2020).

G. Sathyamoorthy, R. Vijay, D. Lenin Singaravelu. Brake friction composite materials: A review on classsifications and influences of friction materials in braking performance with characterizations. Proceeding of the institute of Mechanical Engineers. Part J: Journal of Tribology, Volume 236, Issue 8(2022).

Gai, Peter Friday, Adisa, Ademola Bello, Tokan Aje, Bawa, Mohammed A. Economic viability of basalt based brake pad in Nigeria. International Journal of Engineering Technologies and Management Research. 8(12), 26-41 (2021).

Güney, B., & Mutlu, I. (2019). tribological properties of brake discs coated with cr2o3–40% tio2 by plasma spraying. *Surface Review and Letters*, *26*(10), 1950075.

Hasan Oktem, Ilyas Uygur, Murat Cevik. Design, Construction and Performance of a novel brake pad friction tester. Science direct Volume 115, 2018.

Heerok Hon, Gyeongpil Kim, Junghwan Lee, optimal location of pad for reduction of temperature deviation on brake disc during high-energy braking, journal of mechanical science and technology, 35, 1109-1120 (2021).

J. Abutu, S.A. Lawal, M.B. Ndaliman, R.A. Lafia Araga, O.Adedipe, I.A. Choudhury, Production and characterization of brake pad developed from coconut shell reinforcement material using central composite design, SN Applied Science, (2019) 1:82.

Joseph Abutu, Sunday Albert Lawal, M. B. Ndaliman, Imtiaz Choudhury, Effects of process parameters on the properties of brake pad developed from seashell as reinforcement material using grey relational analysis, Engineering Science and Technology an International Journal 21(4) (2018).

M.I.M. Ahmad, M. Zahri, M.Z. Nuawi, M.F.M. Tabir and M.A. Selamat, Characterization based physical and mechanical properties of brake pad materials for railway vehicle applications, Journal of Materials and Enviroment Science, ISSN: 2028-2508.

Najmuddin M Jamadar and Himmat T Jadhav. A review on braking control and optimization techniques for electric vehicle, Proceedings of the Institution of Mechanical Engineers Part D Journal of Automobile Engineering 235(1):095440702199690 (2021).

Nwogu, C. U and Osarenwinda, J. O. Response Surface Modelling of an Automobile Brake Pad Made from a new- fangled composite material. NIPES Journal of Science and Technology Research 3(3) (2021).

S. S. Lawal, N .A Ademoh, K. C. Bala and A. S. Abdulrahman. A review of the compositions, processing, materials and properties of Brake Pad production. Journal of Physics: Conference series, Volume 1378, Issue 3 (2019).

Yezhe Lyu, Mara Leonard, Jens Wahlstrom, Stefano Gialanella, Ulf Olofsson. Friction wear and airborne particle emission from Cu- free brake materials. Tribology International 141 (2020).

Zeina ammar, hamdy ibrahim, mahmoud adly, ioannis sarris and sherif mehanny. Influence of natural fiber content on the frictional material of brake pads—a review, journal of composite science, and composite 7(1) {2023): 72.